PHYSICAL REVIEW E **93**, 050202(R) (2016)

Faraday wave lattice as an elastic metamaterial

L. Domino, M. Tarpin, S. Patinet, and A. Eddi
Laboratoire de Physique et Mécanique des Milieux Hétérogènes (PMMH), UMR CNRS 7636, PSL-ESPCI, 10 rue Vauquelin, 75005 Paris, France
and Sorbonne Université–UPMC, Université Paris 06, 75005 Paris, France
(Received 25 January 2016; published 19 May 2016)

Metamaterials enable the emergence of novel physical properties due to the existence of an underlying subwavelength structure. Here, we use the Faraday instability to shape the fluid-air interface with a regular pattern. This pattern undergoes an oscillating secondary instability and exhibits spontaneous vibrations that are analogous to transverse elastic waves. By locally forcing these waves, we fully characterize their dispersion relation and show that a Faraday pattern presents an effective shear elasticity. We propose a physical mechanism combining surface tension with the Faraday structured interface that quantitatively predicts the elastic wave phase speed, revealing that the liquid interface behaves as an elastic metamaterial.

DOI: 10.1103/PhysRevE.93.050202

Introduction. An artificial material made of organized subwavelength functional building blocks is called a metamaterial [1,2] when it exhibits properties that differ greatly from that of the unit cell. These new physical properties are intrinsic of the presence of an underlying structure. Although metamaterials are still strongly associated with negative index materials in optics [3], they also refer to structures with mechanical [4], acoustic [5], or even thermodynamic properties [6]. By engineering building blocks from micro to metric scale, several new mechanical properties emerge in metamaterials, such as cloaking in elastic plates [7], auxetic behavior [8,9], ultralight materials [10], or seismic wave control [11]. So far the main challenge has been to design appropriate unit cells to obtain efficient metamaterial constructions. Here, we propose an approach that uses stationary waves to produce the underlying structure of a macroscopic metamaterial.

Spatial patterns arising in systems driven away from equilibrium have been extensively studied over the last two decades [12]. The Faraday instability is often used as a model system in nonlinear physics and the patterns emerging from a vertically vibrated fluid layer are well documented [13–17]. This hydrodynamic instability appears at the interface between two fluids subjected to a vertical oscillation. Above a certain threshold of acceleration a_c, the surface shows a stationary deformation that oscillates at half the excitation frequency. This pattern is both stable in time and regular in space, with a Faraday wavelength λ_F defined by the inviscid gravity-capillary wave dispersion relation

$$\omega_F^2 = \left(gk_F + \frac{\sigma}{\rho}k_F^3\right)\tanh(k_F h), \tag{1}$$

where $k_F = 2\pi/\lambda_F$ is the Faraday wave number, $g = 9.81\ \mathrm{m\,s^{-2}}$ is the acceleration of gravity, σ is the surface tension of the fluid, h the fluid depth, and ρ its density. For specific experimental conditions, one can achieve the formation of well structured and stable patterns (squares, hexagons, triangles... [15]). Although the pattern selection of this instability is quite complex, for a square vessel it is most often a square pattern that is obtained, with its two main directions aligned with the sides of the container. The pattern becomes unstable upon increasing the driving amplitude, and leads to a chaotic state [18] called "defect-mediated turbulence" [19,20]. For the Faraday instability the mechanism of transition to chaos has been studied in [21]. It is found to be achieved by a phase instability called oscillatory transition phase. This oscillatory regime exhibits transverse waves with properties reminiscent to that of waves in an elastic crystalline solid [21]. The same analogy was developed for a square pattern in a vertically oscillating granular layer where phonons have been evidenced [22].

Similar oscillatory motions were observed and characterized in one-dimensional systems such as Faraday instability in an annular cell [23], Taylor-Couette [24], falling liquid columns [25], Rayleigh-Bénard convection rolls [26], and viscous fingering [27]. Very few two-dimensional (2D) systems exhibit this kind of secondary oscillatory modes: liquid columns [28], bouncing droplets crystalline aggregates [29], and vibrated granular materials [22].

In this Rapid Communication, we first characterize the spontaneous in-plane transverse waves that the Faraday structure exhibits. We study their propagation in the 2D structure and link their existence to the emergence of an effective elastic shear modulus of the fluid-air interface confirming previous hypotheses [20,27]. We furthermore propose a physical interpretation that quantifies the appearance of this effective mechanical property revealing that a Faraday wave lattice behaves as an elastic metamaterial.

Experimental setup. Our experimental setup consists of a square vessel (13 cm × 13 cm) filled with a thin layer of silicone oil (viscosity $\eta = 5$ mPa s, density $\rho = 0.965\ \mathrm{kg\,L^{-1}}$, and surface tension $\sigma = 20.9\ \mathrm{mN\,m^{-1}}$) of thickness $h = 3$–5 mm. The vessel is mounted on a vibration exciter (Brüel & Kjær), driven with a computer-controlled amplifier. The acceleration delivered by the vibration exciter is monitored using a calibrated accelerometer. The bath acceleration $a\cos 2\pi f_0 t$ is sinusoidal, with frequency f_0 ranging from 72 to 120 Hz. Above a given threshold acceleration a_c, the liquid interface spontaneously destabilizes and presents a regular square pattern of standing waves [see Fig. 1(a)] with Faraday frequency $f_F = f_0/2$. The size of the pattern is about 25 × 25 Faraday wavelengths. We define the normalized control parameter as $\varepsilon = (a - a_c)/a_c$.

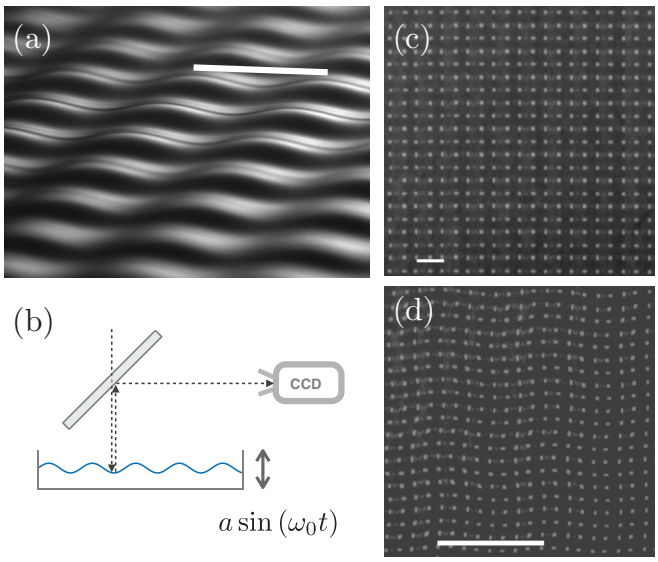

FIG. 1. (a) Side view of the standing Faraday instability wave pattern obtained for $\varepsilon > 0$ at $f_0 = 72$ Hz. The length of the white segment represents the Faraday wavelength (here $\lambda_F = 5.1$ mm). (b) Sketch of the experimental setup. (c) Top view of the stable square pattern. The white segment has a length equal to $\lambda_F = 5.1$ mm. (d) Top view of the oscillating Faraday pattern. The white segment has a length equal to $4\lambda_F = 20.4$ mm, which is the wavelength of the spontaneous oscillations.

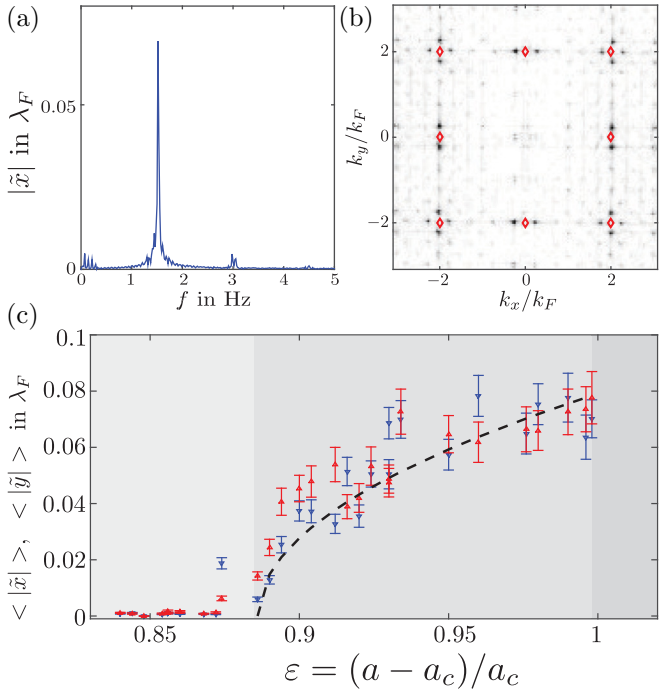

FIG. 2. The forcing frequency is $f_0 = 72$ Hz for this figure. (a) Typical Fourier spectrum $\tilde{x}_{mn}(\omega)$ of the peak (18,18) in the center of the pattern. (b) Modulus of spatial Fourier 2D spectrum $|\hat{y}(k_x,k_y,f)|$ for $\varepsilon = 0.976$, averaged for $f = 1.52 \pm 0.1$ Hz. Open diamonds show the position of the Fourier peaks for a stable pattern [Fig. 1(c)]. (c) Amplitude of the spontaneous vibration as a function of the normalized control parameter, averaged over all the antinodes of the lattice. The up (red) and down (blue) triangles correspond to $|\tilde{y}|$ and $|\tilde{x}|$, respectively. Dashed line is a square root fit. Gray shades denote (from left to right) stable pattern, spontaneous vibrations of the lattice, and chaotic behavior.

The setup and its imaging system are schematically shown in Fig. 1(b). Diffused white light is shone on the container with a uniform square light-emitting diode light and a beam splitter inclined at 45° enables us to image the vessel from the top, using a 2048 × 2048 pixels CCD camera. This imaging technique is the same as presented in [16]. An example of the stable pattern obtained is shown in Fig. 1(c), where only a few wavelengths are represented. This image is obtained by strobing the motion at an appropriate frequency, i.e., 18 Hz when the forcing frequency f_0 is 72 Hz and 30 Hz when the forcing frequency f_0 is 120 Hz. Each white dot corresponds to a horizontal slope of the fluid interface, whether a maximum, a minimum, or a saddle point [16]. There are four white spots per Faraday unit cell [Fig. 1(c)]. Though it does not provide any quantitative information about the wave amplitude in the z direction, we obtain quantitative information about the in-plane location of all the local extrema of the wave pattern.

Spontaneous secondary instability. Upon increasing the driving amplitude to about twice the threshold value, spontaneous oscillations of the square lattice appear [Fig. 1(d) and Supplemental Material movies 1 and 2 [30]]. These oscillations are in-plane modulations of the pattern along its two main directions. They exhibit a spatial periodicity $\lambda = 4\lambda_F$, corresponding to the white segment presented in this figure. We label each bright spot with indices (m,n) and we detect their in-plane position $[x_{mn}(t), y_{mn}(t)]$ using a standard custom MATLAB algorithm. A typical spectrum corresponding to the parameters of Fig. 1(d) is presented in Fig. 2(a). The measured frequency is $f = 1.52$ Hz with an amplitude of $0.07\lambda_F$. To analyze in more detail the spatial structure of the lattice dynamics, we perform spatiotemporal Fourier transforms by carrying out two Fourier analyses, first in time and then in space. The spatial spectrum of the pattern is then computed for each strobed frequency. In Fig. 2(b) we show a typical spatial 2D spectrum obtained at 1.52 ± 0.1 Hz. The Fourier peaks corresponding to the stable Faraday pattern (open diamonds) are split into two symmetric subpeaks indicating the standing nature of the pattern oscillations. These subpeaks are located at a distance $k_f/4$ from the original one, confirming the wavelength selection observed in Fig. 1(d). The peak in the k_x direction (respectively, k_y) is split in the k_y direction (respectively, k_x) revealing that the spontaneous oscillations correspond to the propagation of a standing transverse wave in the initial Faraday square lattice. These spontaneous oscillations of the pattern correspond to a Hopf bifurcation [21] that takes place close to the threshold of transition to chaos. This is confirmed when measuring their amplitude at the vibration frequency as a function of the control parameter ε, where we observe the supercritical nature of this bifurcation [Fig. 2(c)]. This figure also shows that the amplitude of the vibrations is the same for both directions. At $\varepsilon \simeq 1$, the pattern becomes unstable and we observe the formation of defects. We note that this threshold value is different from what was found elsewhere [18,21] as it depends on the depth of the liquid layer, the fluid viscosity, and the forcing frequency.

Here, we want to point out that the spontaneous oscillations occur at a frequency f much lower than the Faraday frequency f_F, whereas their spatial wavelength $\lambda = 2 \pm 0.0012$ cm is four times larger than λ_F. In our experimental conditions and at this frequency f, the gravity-capillary dispersion relation [Eq. (1)] gives a wavelength of $\lambda_{gc} = 23.26$ cm much larger than λ. This means that the transverse standing wave responsible for the pattern oscillations is governed by a different physical mechanism.

Forced vibrations. We now investigate the characteristics of these oscillating modes of the Faraday wave pattern by forcing the vibrations of stable square patterns. We set the Faraday vertical forcing frequency to $f_0 = 120$ Hz (resulting in $\lambda_F = 3.5$ mm), the liquid depth to $h = 3$ mm, and the forcing acceleration to $\varepsilon = 0.81$ in order to get a stable and larger initial Faraday square pattern (its size is now 35×35 Faraday wavelengths). We add to the vessel a custom-made forcing device consisting of a comb dipping into the liquid to a small depth [Fig. 3(a)]. It is mounted so that it is aligned with one side of the container, and it vibrates vertically along with it. The comb is set in motion by a second vibration exciter (Brüel & Kjær) to oscillate horizontally in the reference frame of the container at frequencies ranging from 0.5 to 10 Hz. The distance between the comb teeth is set to $2\lambda_F$, and the amplitude of the forcing sinusoidal motion is set to half the Faraday wavelength. This allows us to generate a sinusoidal oscillation of the line of Faraday peaks located below the forcing comb.

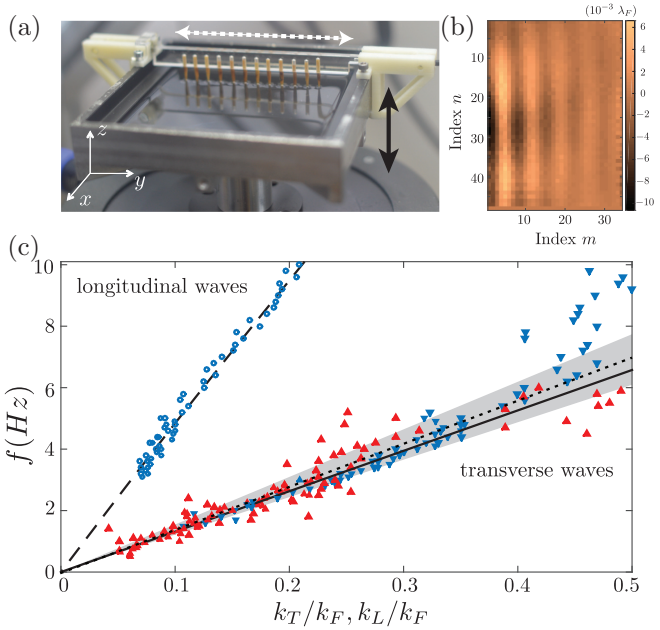

FIG. 3. (a) Device used to force the vibrations of the Faraday pattern. The black arrow shows the vertical motion of the whole vessel, and the dotted white arrow shows the direction of the comb vibration. The width of the vessel is 12 cm. (b) Map of the real part of the fast Fourier transform peak Re($\tilde{y}$) for a forcing frequency of 3.7 Hz and a vertical parametric forcing at $f_0 = 120$ Hz. The forcing device is on the left; each pixel represents a bright point of our images. (c) Dispersion relation $f(k_T)$ and $f(k_L)$. Blue down triangles: transversal waves in the y direction. Red up triangles: transversal waves in the x direction. Open circles: longitudinal waves in the y direction. Solid black line: linear fit. Dashed line: gravity-capillary wave dispersion relation. Dotted line and gray background: prediction from Eq. (4) and its associated uncertainty.

We observe a transversal wave that propagates away from the forcing device at the forcing frequency f. We detect the position $[x_{mn}(t), y_{mn}(t)]$ of each bright spot and perform a temporal Fourier transform to obtain $[\tilde{x}_{mn}(f), \tilde{y}_{mn}(f)]$. Figure 3(b) displays Re$[\tilde{y}(f)]$ for the excitation frequency $f = 3.7$ Hz. We observe a periodic pattern that decays along the x direction (indexed as m) away from the forcing device. This corresponds to the propagation of a transverse wave in the x direction at the forcing frequency f (the motion is along y). The vibration due to this wave is $y(x,t) = y_0 \cos(\phi_y + i2\pi f t)$ and we define the spatial phase ϕ_y of the pattern vibration by $\phi_y(x) = \phi_0 \exp[(-\alpha + ik_T)x]$ where $1/\alpha$ is the decay length of the oscillation and k_T its wave number. From the experimental data we extract α and k_T for each value of f. The decay length $1/\alpha$ does not depend significantly on f and its typical value is $1/\alpha \simeq 11.5\lambda_F$, whereas the value of k_T depends on f. Due to the imperfections of the forcing device, we also notice the presence of a periodicity in the y direction (indexed as n), corresponding to a longitudinal wave propagating in the y direction with wave number k_L that we extract from Fig. 3(b). We perform the same analysis on Re($\tilde{x}$), for which we have similar maps as Fig. 3(b). Altogether, we report the existence of transverse waves along both the x and y directions, as well as longitudinal waves. Figure 3(c) presents the dispersion relations $f(k_T)$ (blue and red triangles) and $f(k_L)$ (open circles) that we obtain for f ranging from 0.5 to 10 Hz. We first notice that $f(k_L)$ obeys the standard surface waves dispersion relation predicted by Eq. (1) (dashed line). This means that the forcing device induces gravity-capillary waves. Their dispersion relation appears quite linear in Fig. 3(c) since the shallow water approximation applies ($k_F h \ll 1$). On the other hand, the dispersion relation for transverse waves $f(k_T)$ is markedly different. We observe a linear increase of f with k_T with a much lower slope. A linear fit gives the phase speed of the transverse waves $c_T = 4.60$ cm s^{-1}.

Physical interpretation. These experimental results show that there exists a new type of wave propagating at the fluid-air interface. They are transverse waves associated to the presence of a preexisting Faraday wave pattern and reminiscent of 2D shear waves that propagate in elastic media. Here we present a quasi-2D model in which we identify the Faraday cellular pattern to a 2D metamaterial with solidlike properties. Indeed, transverse waves in an elastic material propagate with constant phase velocity c_T that only depends on the elastic shear modulus μ. We use the structure of the Faraday wave lattice and the fluid properties to derive an effective elastic shear modulus and quantitatively predict the transverse waves properties.

We consider a reference state for the interface defined as

$$z_0(x,y,t) = A(t) \cos\left(\pi \frac{x+y}{\lambda_F}\right) \cos\left(\pi \frac{x-y}{\lambda_F}\right), \qquad (2)$$

with $A(t) = A_0 \cos(2\pi f_F t)$ the amplitude of the stationary wave. Measurements [e.g., in Fig. 1(a)] give $A_0/\lambda_F = 13.5\% \pm 3.5\%$. This 2D function gives a succession of peaks and crests arranged in a square pattern, as represented in

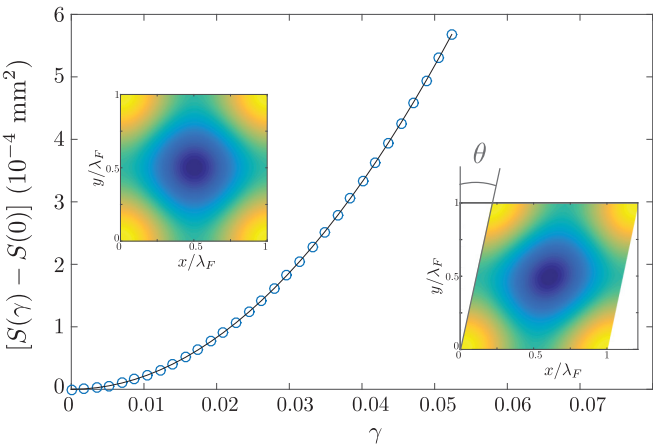

FIG. 4. Open circles: evolution of $S(\gamma)$ with γ computed numerically for $\lambda_F = 3.5$ mm and $A_0/\lambda_F = 13.5\%$. Dark line: theoretical prediction from Eq. (3). Inset (left): reference surface. Inset (right): sheared surface, with $\tan\theta = \gamma$.

Fig. 4 (inset on the left). We apply a shear strain $\gamma = \tan\theta$ to this elementary cell [Fig. 4 (inset on the right)] and calculate analytically its surface area $S(\gamma)$:

$$S(\gamma) = \int_0^{\lambda_F} dy \int_{\gamma y}^{\lambda_F+\gamma y} dx \times \left[1 + \left(\frac{\partial z_0}{\partial x}\right)^2 + \left(\frac{\partial z_0}{\partial y} - \gamma\frac{\partial z_0}{\partial x}\right)^2\right]^{1/2}. \quad (3)$$

As $f \ll f_F$ we average $S(\gamma)$ in time which corresponds to replacing $A(t)$ with $\mathcal{A} = A_0 2/\pi$. Figure 4 shows the numerical evaluation of $S(\gamma)$ for $A_0/\lambda_F = 13.5\%$.

As $S(\gamma)$ is an even function (γ and $-\gamma$ give the same area), $\frac{\partial S}{\partial \gamma}|_{\gamma=0} = 0$. For a nonzero amplitude of the Faraday wave, the shearing deformation leads to a surface excess $\Delta S = S(\gamma) - S(0)$ that we can approximate for small deformations

$$\Delta S = \frac{1}{2}\frac{\partial^2 S}{\partial \gamma^2}\bigg|_{\gamma=0}\gamma^2 = \frac{1}{2}S_{\gamma\gamma}\gamma^2.$$

For our experimental parameters ($\lambda_F = 3.5$ mm and $A_0/\lambda_F = 13.5\%$) we obtain $S_{\gamma\gamma} \simeq 4.13 \times 10^{-7}$ mm^2.

Due to surface tension there is an energy cost that depends on the applied shear deformation $\Delta E(\gamma) = \sigma \Delta S(\gamma)$. We then define the effective elastic energy density per unit area $W_S = \sigma \Delta S/\lambda_F^2$ (in J m^{-2}) and introduce the effective shear modulus μ_S of the Faraday wave pattern: $W_S = 2\mu_S \epsilon_{xy}^2$ where $\epsilon_{xy} = \frac{1}{2}\gamma$. Following standard elasticity theory [31] the transverse elastic wave phase velocity c_T in a 2D elastic medium is written

$$c_T = \sqrt{\frac{\mu_S}{\rho_S}} = \sqrt{\frac{\sigma S_{\gamma\gamma}}{\rho_S \lambda_F^2}}, \quad (4)$$

with ρ_S the density per unit area, defined as $\rho_S = \rho\mathcal{A}$.

Using Eqs. (2) and (3), the velocity we obtain is $c_T = 4.84 \pm 0.63$ cm s^{-1}, which is in excellent agreement with the experimental result of 4.60 cm s^{-1}. We represent in Fig. 3(c) the estimated dispersion relation (dotted line), with the gray background representing the uncertainty.

Conclusion. We have characterized a secondary instability that arises in 2D Faraday patterns close to the transition towards chaos. This instability leads to vibrations of the Faraday pattern similar to a 2D transverse elastic wave which confirms previous observations [21,22]. We established the dispersion relation for these waves and showed that it differs markedly from the standard gravity-capillary waves that propagate at the liquid-air interface. We propose a physical mechanism that combines the surface tension with the preexisting Faraday wave structure at the interface. We are able to derive an effective shear modulus μ_S for the Faraday wave pattern that quantitatively agrees with the experimental observations.

In this work, we observe the emergence of a new physical property, namely, an effective 2D shear elasticity, at the liquid-air interface. This effective elasticity was identified with granular materials [22] and with liquids [21] submitted to vertical vibrations. In all cases common features can be found such as the emergence of transverse modes, decoupling in time (between forcing frequency f_0 and vibration frequency f) and in space (between lattice wavelength λ_F and vibration wavelength λ), and many quantitative observations are about the same order of magnitude. Nevertheless, some important differences should be noted: in [22], the dispersion branch flattens close to the edge of the first Brillouin zone and the transverse modes appear along the (1,1) direction of the 2D lattice, whereas here and in [21] the (1,0) mode is excited. In [21], the authors observe a single mode, whereas we are able to establish the entire dispersion relation thanks to our forcing device.

We also present a model based on surface tension that accounts for our experimental observations. Our description using surface tension is not applicable to granular materials used in [22] and the two systems should be compared with caution. We believe our description of the pattern as a metamaterial could apply to the data from [21]. Our interpretation reveals that the effective elasticity is intimately related to the existence of a periodic pattern imprinted on the liquid interface. From this perspective, the Faraday wave pattern creates a mechanical metamaterial at macroscopic scale.

In the future, we would like to investigate in more detail the limit $k/k_F = 1/2$ corresponding to the edge of the first Brillouin zone in a crystalline material. Another line of future research is to understand if there exists a second elastic constant for the medium as in usual elastic solids. More generally, wave-based metamaterials offer unique possibilities as wavelengths and patterns can be dynamically tuned.

Acknowledgments. The authors would like to thank E. Fort and Y. Couder for fruitful discussions as well as X. Benoit-Gonin and A. Fourgeaud for their help in setting up the experiments.

[1] J. B. Pendry, D. Schurig, and D. R. Smith, Science **312**, 1780 (2006).

[2] M. Kadic, T. Bückmann, R. Schittny, and M. Wegener, Rep. Prog. Phys. **76**, 126501 (2013).

[3] J. B. Pendry, Phys. Rev. Lett. **85**, 3966 (2000).
[4] B. Florijn, C. Coulais, and M. van Hecke, Phys. Rev. Lett. **113**, 175503 (2014).
[5] F. Lemoult, N. Kaina, M. Fink, and G. Lerosey, Nat. Phys. **9**, 55 (2013).
[6] R. Schittny, M. Kadic, S. Guenneau, and M. Wegener, Phys. Rev. Lett. **110**, 195901 (2013).
[7] N. Stenger, M. Wilhelm, and M. Wegener, Phys. Rev. Lett. **108**, 014301 (2012).
[8] T. Bückmann, R. Schittny, M. Thiel, M. Kadic, G. W. Milton, and M. Wegener, New J. Phys. **16**, 033032 (2014).
[9] T. Bückmann, N. Stenger, M. Kadic, J. Kaschke, A. Frölich, T. Kennerknecht, C. Eberl, M. Thiel, and M. Wegener, Adv. Mater. **24**, 2710 (2012).
[10] T. A. Schaedler, A. J. Jacobsen, A. Torrents, A. E. Sorensen, J. Lian, J. R. Greer, L. Valdevit, and W. B. Carter, Science **334**, 962 (2011).
[11] S. Brûlé, E. H. Javelaud, S. Enoch, and S. Guenneau, Phys. Rev. Lett. **112**, 133901 (2014).
[12] M. C. Cross and P. C. Hohenberg, Rev. Mod. Phys. **65**, 851 (1993).
[13] M. Faraday, Philos. Trans. R. Soc. London **121**, 299 (1831).
[14] T. B. Benjamin and F. Ursell, Proc. R. Soc. London, Ser. A **225**, 505 (1954).
[15] S. Douady and S. Fauve, Europhys. Lett. **6**, 221 (1988).
[16] S. Douady, J. Fluid Mech. **221**, 383 (1990).
[17] K. Kumar and L. S. Tuckerman, J. Fluid Mech. **279**, 49 (1994).
[18] N. B. Tufillaro, R. Ramshankar, and J. P. Gollub, Phys. Rev. Lett. **62**, 422 (1989).
[19] I. Rehberg, S. Rasenat, and V. Steinberg, Phys. Rev. Lett. **62**, 756 (1989).
[20] P. Coullet, L. Gil, and J. Lega, Phys. Rev. Lett. **62**, 1619 (1989).
[21] I. Shani, G. Cohen, and J. Fineberg, Phys. Rev. Lett. **104**, 184507 (2010).
[22] D. I. Goldman, M. D. Shattuck, S. J. Moon, J. B. Swift, and H. L. Swinney, Phys. Rev. Lett. **90**, 104302 (2003).
[23] S. Douady, S. Fauve, and O. Thual, Europhys. Lett. **10**, 309 (1989).
[24] C. D. Andereck, S. S. Liu, and H. L. Swinney, J. Fluid Mech. **164**, 155 (1986).
[25] F. Giorgiutti, A. Bleton, L. Limat, and J. E. Wesfreid, Phys. Rev. Lett. **74**, 538 (1995).
[26] M. Dubois, R. Da Silva, F. Daviaud, P. Berge, and A. Petrov, Europhys. Lett. **8**, 135 (1989).
[27] L. Bellon, L. Fourtune, V. T. Minassian, and M. Rabaud, Phys. Rev. E **58**, 565 (1998).
[28] C. Pirat, C. Mathis, P. Maïssa, and L. Gil, Phys. Rev. Lett. **92**, 104501 (2004).
[29] A. Eddi, A. Boudaoud, and Y. Couder, Europhys. Lett. **94**, 20004 (2011).
[30] See Supplemental Material at http://link.aps.org/supplemental/10.1103/PhysRevE.93.050202 for movies of the spontaneous instability. Supplementary movie 1: Stroboscopic side view of the spontaneous secondary instability. Supplementary movie 2: Stroboscopic top view of the spontaneous secondary instability. Spatial scales are indicated in the movie.
[31] L. D. Landau and E. M. Lifshitz, *Theory of Elasticity*, 3rd ed. (Butterworth-Heinemann, Oxford, 1986), pp. 87–107.